

Cite this: *Nanoscale*, 2018, **10**, 5617

## Efficient and ultraviolet durable planar perovskite solar cells *via* a ferrocenecarboxylic acid modified nickel oxide hole transport layer†

Jiankai Zhang,<sup>‡a</sup> Hui Luo,<sup>‡a</sup> Weijia Xie,<sup>‡a</sup> Xuanhuai Lin,<sup>a</sup> Xian Hou,<sup>a</sup> Jianping Zhou,<sup>\*b</sup> Sumei Huang,<sup>id a</sup> Wei Ou-Yang,<sup>id a</sup> Zhuo Sun<sup>a</sup> and Xiaohong Chen<sup>id \*a</sup>

Planar perovskite solar cells (PSCs) that use nickel oxide (NiO<sub>x</sub>) as a hole transport layer have recently attracted tremendous attention because of their excellent photovoltaic efficiencies and simple fabrication. However, the electrical conductivity of NiO<sub>x</sub> and the interface contact properties of the NiO<sub>x</sub>/perovskite layer are always limited for the NiO<sub>x</sub> layer fabricated at a relatively low annealing temperature. Ferrocenedicarboxylic acid (FDA) was firstly introduced to modify a p-type NiO<sub>x</sub> hole transport layer in PSCs, which obviously improves the crystallization of the perovskite layer and hole transport and collection abilities and reduces carrier recombination. PSCs with a FDA modified NiO<sub>x</sub> layer reached a PCE of 18.20%, which is much higher than the PCE (15.13%) of reference PSCs. Furthermore, PSCs with a FDA interfacial modification layer show better UV durability and a hysteresis-free effect and still maintain the original PCE value of 49.8% after being exposed to UV for 24 h. The enhanced performance of the PSCs is attributed to better crystallization of the perovskite layer, the passivation effect of FDA, superior interface contact at the NiO<sub>x</sub>/perovskite layers and enhancement of the electrical conductivity of the FDA modified NiO<sub>x</sub> layer. In addition, PSCs with FDA inserted at the interface of the perovskite/PCBM layers can also improve the PCE to 16.62%, indicating that FDA have dual functions to modify p-type and n-type carrier transporting layers.

Received 23rd November 2017,

Accepted 13th February 2018

DOI: 10.1039/c7nr08750k

rsc.li/nanoscale

## 1. Introduction

Perovskite solar cells (PSCs) have attracted growing attention because of their promising advantages of low-cost and high efficiency. Although the power conversion efficiency of the mesoporous PSCs is already more than 22.7%,<sup>1</sup> high temperature processing at 500 °C is still required for the most efficient mesoporous PSCs. Planar structured perovskite solar cells compared to the mesoporous PSCs are expected to be popular due to their simple fabrication. The emergent inverted (p-i-n) planar PSCs consist of a methyl ammonium lead halide perovskite which is usually sandwiched between the electron/hole selective layers to facilitate charge extraction. Poly(3,4-ethylene-dioxythiophene)-polystyrene sulfonate (PEDOT:PSS) as a hole

buffer layer has been widely applied in inverted PSCs.<sup>2</sup> However, PEDOT:PSS strongly limits the lifetime and performance of cells due to its hydroscopic and acidic nature along with its inability to block electrons.<sup>2,3</sup>

Inorganic p-type semiconductors, such as CuSCN,<sup>4</sup> CuI<sup>5</sup> and CoO<sub>x</sub><sup>6</sup> as a hole transport layer (HTL) instead of PEDOT:PSS have better stability for PSCs. The typical nickel oxide (NiO<sub>x</sub>) as an HTL has shown great potential due to its large band gap and deep valence band.<sup>7,8</sup> Jen *et al.*<sup>9</sup> used a solution-processed copper-doped nickel oxide as an HTL to improve electrical conductivity, which greatly enhanced the PCE of PSCs from 8.94% to 15.40%. Recently, the Li<sup>+</sup>/Mg<sup>2+</sup> co-doped NiO<sub>x</sub> as an HTL has been developed by Chen *et al.*,<sup>10</sup> where PSCs obtained a PCE of 16.2% with a square centimeter area. However, high temperature processing at 400 °C is still required to obtain high conductivity of NiO<sub>x</sub> and thus superior performance of PSCs.<sup>11</sup> NiO<sub>x</sub> as a hole transport layer using low temperature treatment is one of the most interesting aspects. But NiO<sub>x</sub> with low temperature processing usually suffers from a series of deficiencies such as reduced carrier transport and extraction abilities, enhanced carrier recombination and a hysteresis effect due to its increasing defects and inferior crystallinity.<sup>12</sup> The preformed nano-crystals of NiO<sub>x</sub> as

<sup>a</sup>Engineering Research Center for Nanophotonics and Advanced Instrument, Ministry of Education, and School of Physics and Materials Science, East China Normal University, Shanghai 200062, China. E-mail: xhchen@phy.ecnu.edu.cn

<sup>b</sup>School of Automation Engineering, Shanghai University of Electric Power, Shanghai 200090, China. E-mail: zhoujianping@shiep.edu.cn

†Electronic supplementary information (ESI) available. See DOI: 10.1039/c7nr08750k

‡First co-authors.

the HTL with a low-temperature process were reported to be an efficient way to improve efficiency and inhibit the hysteresis effect of the PSCs.<sup>13</sup> The sol-gel fabricated NiO<sub>x</sub> films with a relatively low temperature treatment usually need to use a surface modification method to improve the contact properties between the perovskite and hole transport layers.<sup>14</sup> Yang *et al.*<sup>14</sup> employed diethanolamine to modify the NiO<sub>x</sub> surface, which obviously improves the efficiency and reduce the hysteresis effect due to the superior NiO<sub>x</sub>/perovskite contact and perovskite crystallization. Although the origin of the hysteresis effect in PSCs still needs to be investigated, some factors such as slow trapping or detrapping of charges in electronic interface states,<sup>15</sup> contact conductivity,<sup>16</sup> ferroelectricity<sup>17</sup> and ion migration,<sup>18</sup> can all result in the hysteresis effect of the PSCs.

Ferrocene derivatives have been widely used in the fields of catalysts,<sup>19</sup> electrochemistry,<sup>20</sup> and organic solar cells<sup>21</sup> due to their unique chemical structure, high thermal stability and chemical stability. The ferrocenedicarboxylic acid is inserted between ITO and n-type ZnO as a modified layer, which successfully improves the PCE of organic solar cells due to enhanced exciton dissociation and charge collection efficiencies.<sup>21</sup> In this paper, we firstly introduced ferrocenedicarboxylic acid (FDA) as a p-type NiO<sub>x</sub> interfacial modified layer, which can overcome the inferior contact properties and high density defects of the NiO<sub>x</sub> interface. The PCE of PSCs modified with FDA is significantly increased to 18.20% from 15.13% with reference cells, and its hysteresis is eliminated. Furthermore, PSCs with FDA show better UV-resistance. The enhanced performance of PSCs with FDA is attributed to better crystallization of the perovskite, superior interface contact at the NiO<sub>x</sub>/perovskite layers, the passivation effect of FDA and enhancement of the electrical conductivity of the FDA modified NiO<sub>x</sub> layer.

## 2. Experimental section

FDA (purchased from Sinopharm Chemical Reagent) powders were dispersed in chlorobenzene, and stirred at room temperature for 12 h. The chemical structure of FDA is shown in Fig. S1.† A perovskite precursor solution was prepared by dissolving 1 M methyl ammonium iodide (MAI, purchased from 1-Material Inc.) and 1 M lead(II) iodide (PbI<sub>2</sub>, 99.9%, Aladdin Reagents) in a mixture of dimethyl sulphoxide (DMSO, AR 99% GC, Aladdin Reagents) and  $\gamma$ -butyrolactone (GBL, AR 99% GC, Aladdin Reagents) (7 : 3 v/v). The pre-cleaned ITO coated glass with a sheet resistance of 10  $\Omega$   $\square^{-1}$  was treated with ultraviolet ozone for 20 minutes. NiO<sub>x</sub> solutions were spin-coated at 4500 rpm for 1 min to form a 20 nm thick film, followed by annealing at 235 °C for 45 min. The NiO<sub>x</sub> solution was prepared by dissolving 25 mg nickel acetate tetrahydrate in 1 ml 2-methoxyethanol and 6  $\mu$ l monoethanolamine. Then the FDA solution was spin-coated onto the surface of the NiO<sub>x</sub> layer at 4000 rpm for 1 min in a N<sub>2</sub>-filled glove box. Next, the samples were retained for 30 min before spin-coating the perovskite layer further. The CH<sub>3</sub>NH<sub>3</sub>PbI<sub>3</sub> film was spin-coated on NiO<sub>x</sub>

or the FDA modified NiO<sub>x</sub> layer by a consecutive two-step spin-coating process at 2000 rpm and 4000 rpm for 20 s and 60 s, respectively. During the second spin-coating step, chlorobenzene drop-casting was employed to replace DMSO solvent. The samples were dried at 100 °C for 10 minutes. After being cooled down, a 40 nm thick PCBM ([6,6]-phenyl-C 61-butyric acid methyl ester) layer was formed onto the CH<sub>3</sub>NH<sub>3</sub>PbI<sub>3</sub> film by spin-coating the PCBM solution dissolved in chlorobenzene (10 mg mL<sup>-1</sup>) at 1200 rpm for 60 s. Finally, a 100 nm thick AgAl alloy electrode was thermally evaporated onto the PCBM layer under a base pressure of 5  $\times$  10<sup>-4</sup> Pa. The weight ratio (wt%) of Al to Ag in the AgAl alloy, purchased from Trillion Metals Co., Ltd (Beijing, China), is 3 wt%. The fabrication process of polymer solar cells is as follows. PTB7-Th (99%) was purchased from 1-Material Inc. and PC71BM (99.5%) was purchased from Solenne BV. A blend solution containing PTB7-Th:PC71BM (7 mg mL<sup>-1</sup>:10.5 mg mL<sup>-1</sup>) dissolved in chlorobenzene/1,8-diiiodooctane (97 : 3, v/v) at 1000 rpm for 15 s was spin-coated onto an AZO surface to form an 80 nm photoactive layer. A 7 nm thick MoO<sub>3</sub> interlayer and a 100 nm AgAl alloy electrode were then thermally evaporated onto the active layer.

The surface morphologies of the samples were investigated by field-emission scanning electron microscopy (SEM, Hitachi S-4800) and Atomic Force Microscopy (AFM, JPK Nano Wizard II), respectively. The X-ray diffraction (XRD) patterns of the perovskite films were recorded with an PW3040/60 instrument (Holland Panalytical PRO) using a Cu K $\alpha$  radiation source ( $V = 30$  kV,  $I = 25$  mA). Photoluminescence (PL) spectra were recorded using a fluorescence spectrophotometer (HORIBA Jobin Yvon Fluoromax-4). The transmission and absorption spectra of the samples were recorded using a UV-Vis spectrophotometer (Hitachi U-3900). The current density-voltage ( $J$ - $V$ ) characteristics were measured using a Keithley model 2440 source meter in a Newport solar simulator system with an AM1.5G filter and 100 mW cm<sup>-2</sup> illumination calibrated by using a standard silicon reference cell (Newport Oriel Instruments 91150V). The incident photon to current conversion efficiency (IPCE) spectra were recorded using a Newport Optical Power Meter 2936-R by illuminating the device with monochromatic light supplied from a xenon arc lamp in combination with a dual-grating monochromator. The reference numbers of photons incident on the sample were calibrated for each wavelength using a silicon photodiode (Newport Oriel Instruments 71675-71580). EIS measurements were recorded in the dark in the frequency range from 0.1 to 1  $\times$  10<sup>6</sup> Hz using an Autolab PGSTAT 302N electrochemical workstation. The thickness of the NiO<sub>x</sub> film was measured by using the DEKTAK XT stylus profiler.

## 3. Results and discussion

Similar SEM images of NiO<sub>x</sub> modified without and with FDA were observed, as shown in Fig. 1(a and b). The surface root-mean-square roughness (RMS) of NiO<sub>x</sub>/FDA and NiO<sub>x</sub> is respectively 5.57 nm and 8.01 nm, as shown in Fig. 1(c and d),

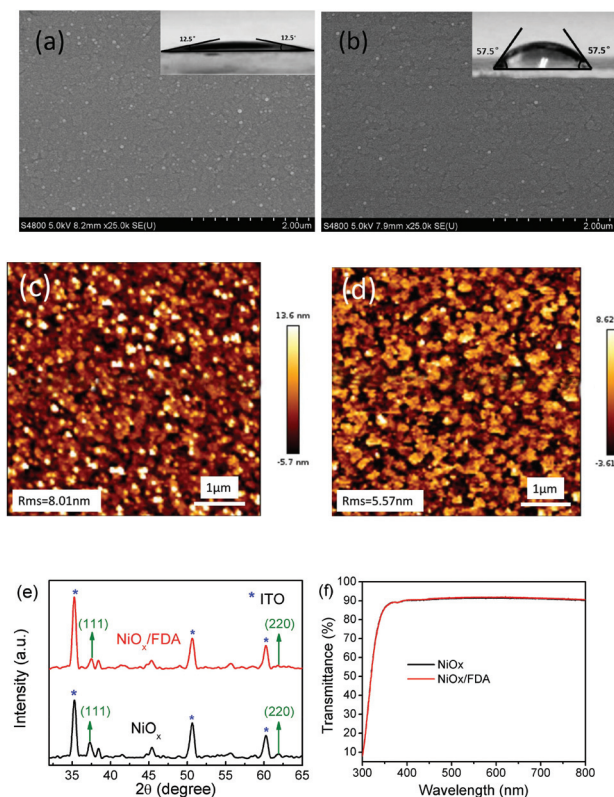


**Fig. 1** SEM images of the NiO<sub>x</sub> surface modified without (a) and with (b) an FDA interfacial layer; AFM images of the NiO<sub>x</sub> surface modified without (c) and with (d) the FDA layer; (e) XRD patterns of NiO<sub>x</sub>/FDA and NiO<sub>x</sub> films onto ITO-coated glass; (f) transmittance spectra of NiO<sub>x</sub>/FDA and NiO<sub>x</sub> films onto a glass substrate. The FDA concentration of the modified NiO<sub>x</sub> surface is 0.1 mg ml<sup>-1</sup>.

indicating that the surface NiO<sub>x</sub> modified with FDA becomes smoother. Meanwhile, the contact angle of the NiO<sub>x</sub> surface modified with FDA compared to the pristine NiO<sub>x</sub> surface was increased to 57.5° from 12.5°. The reduced surface roughness and the improved contact angle of the NiO<sub>x</sub>/FDA surface are beneficial to reduce the perovskite nuclei density,<sup>22,23</sup> helping to form larger sized perovskite grains.<sup>24</sup> The X-ray diffraction (XRD) patterns of the corresponding NiO<sub>x</sub> films are shown in Fig. 1e. The diffraction peaks at 37.24° and 62.86° are assigned to the typical diffractions of the (111) and (220) planes of the NiO<sub>x</sub>.<sup>25</sup> The XRD curves of the NiO<sub>x</sub> modified with and without FDA are almost similar, indicating that FDA modification did not obviously change the structure of the NiO<sub>x</sub> layer. The similar transmittance spectra of the NiO<sub>x</sub> films modified with and without FDA were observed, as shown in Fig. 1f, which is consistent with the previous report,<sup>26,27</sup> indicating that the enhanced PCE and UV-resistance of PSCs are not related to the acceptance dose of UV-visible light.

Fig. 2a and b show the surface morphologies of the perovskite films on NiO<sub>x</sub> modified without and with the FDA layer. The grain sizes of the perovskite layer onto NiO<sub>x</sub>/FDA compared to the pristine NiO<sub>x</sub> substrate become obviously larger, which can be further demonstrated from X-ray diffraction

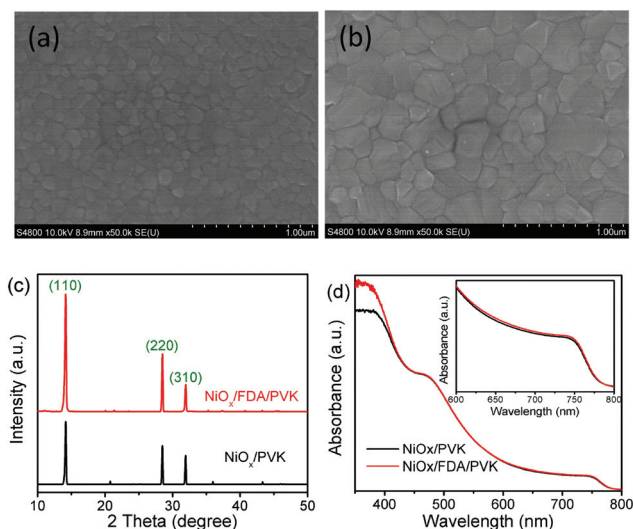


**Fig. 2** SEM images of the perovskite layer on (a) NiO<sub>x</sub> and (b) NiO<sub>x</sub>/FDA films; (c) XRD patterns and (d) UV-Vis absorption spectra of perovskite (PVK) films on the NiO<sub>x</sub> and NiO<sub>x</sub>/FDA layer, respectively. The FDA concentration of the spin-coated NiO<sub>x</sub> surface is 0.1 mg ml<sup>-1</sup>.

(XRD) patterns, as shown in Fig. 2c. The strong peaks at 14.12°, 28.48° and 31.86° correspond to the (110), (220) and (310) planes of the perovskite films. The intensities of these three peaks are obviously increased for the perovskite layer grown on the FDA modified NiO<sub>x</sub> layer. In the meantime, the absorbance of the perovskite layer onto the NiO<sub>x</sub>/FDA substrate is slightly increased due to the better crystallinity of the perovskite,<sup>28</sup> as shown in Fig. 2d. These results suggested that the FDA modified NiO<sub>x</sub> surface can improve the crystallization of the perovskite layer, which helps to reduce carrier recombination and improve the photocurrent of the PSCs.

The *J*-*V* curves of the PSCs based on NiO<sub>x</sub> modified with different FDA concentrations are shown in Fig. S2.† The photovoltaic parameters of the PSCs are summarized in Table S1.† The optimized FDA concentration spin-coated onto the NiO<sub>x</sub> surface is 0.1 mg ml<sup>-1</sup>. The *J*-*V* characteristics of typical PSCs based on NiO<sub>x</sub> with and without the FDA modified layer are shown in Fig. 3a. The improved PCE of the PSCs modified with FDA is primarily attributable to the higher *J*<sub>sc</sub> and FF. PSCs without FDA modification achieved a PCE = 14.77% with a *J*<sub>sc</sub> = 20.2 mA cm<sup>-2</sup>, *V*<sub>oc</sub> = 1.02 V, FF = 71.7% under a forward scan, and a PCE of 14.46% with a *J*<sub>sc</sub> of 20.2 mA cm<sup>-2</sup>, a *V*<sub>oc</sub> of 1.02 V and an FF of 70.2% under a reverse scan. The hysteresis effect of the reference PSCs was obviously observed. However, PSCs with FDA modification showed a PCE of 17.87% with *J*<sub>sc</sub> = 22.55 mA cm<sup>-2</sup>, *V*<sub>oc</sub> = 1.04 V, and FF = 76.2% at a forward scan and a PCE of 17.59% with *J*<sub>sc</sub> = 22.53 mA cm<sup>-2</sup>, *V*<sub>oc</sub> = 1.04 V and FF = 75.8% at a reverse scan, indicating a negligible hysteresis effect. The PCE distributions for 40 devices with and without FDA modification are shown in Fig. 3b. The highest PCEs of PSCs with and without FDA are 18.20% and 15.13%, respectively. The obviously higher PCE and more narrow distributions of PSCs with FDA modification indicate that PSCs

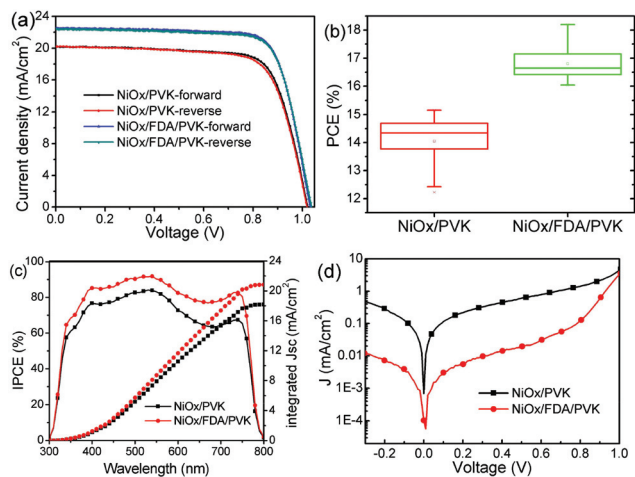


**Fig. 3** (a)  $J$ - $V$  characteristics of PSCs with and without FDA modification under forward and reverse scans with a  $100 \text{ mV s}^{-1}$  rate; (b) statistical PCEs of 40 devices with  $\text{NiO}_x/\text{PVK}$  and  $\text{NiO}_x/\text{FDA}/\text{PVK}$ ; (c) IPCE curves and (d) dark  $J$ - $V$  curves of PSCs with and without FDA modification. The FDA concentration of the spin-coated  $\text{NiO}_x$  surface is  $0.1 \text{ mg ml}^{-1}$ .

with FDA modification have better performance and reproducibility. The incident photon to current conversion efficiency (IPCE) curves in the wavelength range from 350 nm to 750 nm of PSCs with FDA modification are obviously higher than those of the reference PSCs, as shown in Fig. 3c, which is partly attributed to the better crystallinity of the perovskite grown on FDA modified  $\text{NiO}_x$ . The improved carrier transport and extraction abilities can also improve the IPCE values, especially in the red wavelength portion because a higher number of photons are distributed in the wavelength range from 600 to 800 nm.<sup>29</sup> The integrated  $J_{\text{sc}}$  values from the IPCE spectra of PSCs with and without FDA are respectively  $20.9 \text{ mA cm}^{-2}$  and  $18.2 \text{ mA cm}^{-2}$ , which are somewhat lower than  $J_{\text{sc}}$  values from the  $J$ - $V$  curves. This is probably attributed to the defects of cells and part deviation of the IPCE measurement.<sup>30,31</sup> The dark  $J$ - $V$  curves of PSCs with and without FDA modification are shown in Fig. 3d. The reverse saturation current is obviously decreased and the rectifying property is improved for cells with FDA. This means that the carrier recombination is reduced and the charge accumulation phenomenon is weakened at the  $\text{NiO}_x$ /perovskite interface due to the modification of FDA, which is helpful to improve the FF and  $J_{\text{sc}}$  of PSCs.<sup>30,32</sup>

The steady-state photoluminescence (PL) spectra were widely investigated to gain insight into the photo-physical properties of the perovskite. The PL intensity of the perovskite film is related to carrier recombination and carrier transport and extraction abilities at the interface between the perovskite and carrier transport layers.<sup>33</sup> Fig. 4a shows the steady-state photoluminescence (PL) spectra of the perovskite layer spin-coated onto the  $\text{NiO}_x$  and  $\text{NiO}_x/\text{FDA}$  surface. The PL intensity of the perovskite onto  $\text{NiO}_x/\text{FDA}$  compared to pure  $\text{NiO}_x$  was greatly quenched, suggesting that carriers can be quickly transferred from the perovskite to the  $\text{NiO}_x$  layer using

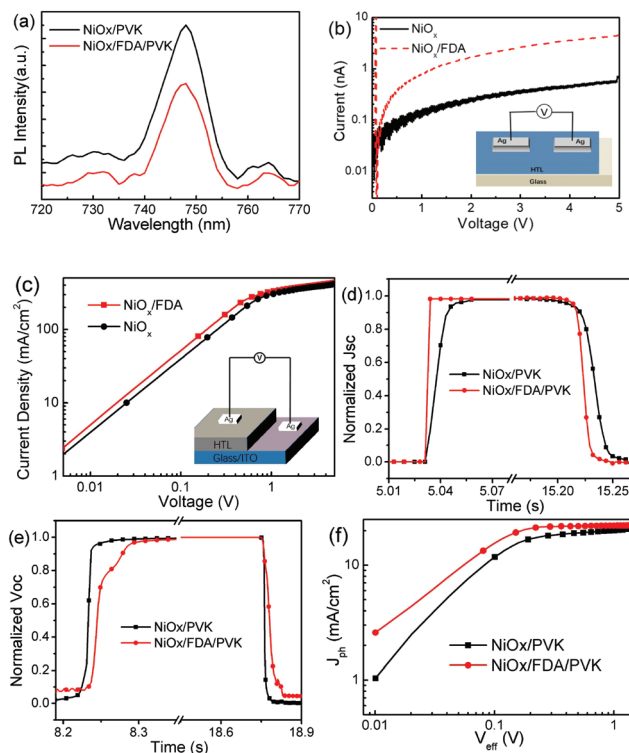


**Fig. 4** (a) Photoluminescence of perovskite films on top of  $\text{NiO}_x$  and  $\text{NiO}_x/\text{FDA}$ ;  $I$ - $V$  curves of  $\text{NiO}_x$  and  $\text{NiO}_x/\text{FDA}$  films from parallel (b) and vertical (c) directions and the insets are the schematic diagram of the testing structure; transient (d)  $J_{\text{sc}}$  and (e)  $V_{\text{oc}}$  response curves of PSCs with and without FDA modification; (f) plots of  $J_{\text{ph}}$  versus  $V_{\text{eff}}$  for cells based on  $\text{NiO}_x$  modified with and without FDA.

FDA modification. The  $I$ - $V$  curves of the  $\text{NiO}_x$  and  $\text{NiO}_x/\text{FDA}$  layers from parallel and vertical directions were further measured, as shown in Fig. 4b and c. The enhanced current of the  $\text{NiO}_x/\text{FDA}$  layer from the vertical direction indicates that FDA modification helps carrier extraction, which is consistent with the stronger PL quenching of the perovskite deposited onto the  $\text{NiO}_x/\text{FDA}$  layer. Furthermore, the current difference of the  $\text{NiO}_x/\text{FDA}$  film compared to pure  $\text{NiO}_x$  can be further enlarged in the parallel direction, indicating that FDA modification helps to improve the conductivity of the  $\text{NiO}_x$  layer. Fig. 4(d and e) show the transient  $J_{\text{sc}}$  and  $V_{\text{oc}}$  profiles of PSCs, respectively. The quickly increasing  $J_{\text{sc}}$  and a slower decay of  $V_{\text{oc}}$  for PSCs with FDA modification indicate reduced trap states at the interface of the perovskite/ $\text{NiO}_x$  layers.<sup>34,35</sup> Fig. 4f reveals the effect of FDA modification on the photocurrent density ( $J_{\text{ph}}$ ) versus effective voltage ( $V_{\text{eff}}$ ).  $J_{\text{ph}}$  is determined as  $J_{\text{ph}} = J_{\text{light}} - J_{\text{dark}}$ , where  $J_{\text{light}}$  and  $J_{\text{dark}}$  are the current density under illumination and in the dark, respectively.  $V_{\text{eff}}$  is determined as  $V_{\text{eff}} = V_0 - V_a$ , where  $V_0$  is the voltage at which  $J_{\text{ph}} = 0$  and  $V_a$  is the applied bias voltage.  $J_{\text{ph}}$  increases linearly at a low  $V_{\text{eff}}$  and saturates at a high  $V_{\text{eff}}$ . In general, the saturated photocurrent ( $J_{\text{sat}}$ ) is correlated to the maximum exciton generation rate ( $G_{\text{max}}$ ), exciton dissociation probability, and carrier transport and collecting probability in a high  $V_{\text{eff}}$  region.<sup>29,36</sup>

$G_{\max}$  could be obtained as  $J_{\text{ph}} = qG_{\max}L$ , where  $q$  is the electronic charge and  $L$  is the thickness of the perovskite film (140 nm). The values of  $G_{\max}$  for devices with and without FDA modification are  $9.92 \times 10^{27} \text{ m}^{-3} \text{ s}^{-1}$  ( $J_{\text{sat}} = 222.6 \text{ A m}^{-2}$ ) and  $9.62 \times 10^{27} \text{ m}^{-3} \text{ s}^{-1}$  ( $J_{\text{sat}} = 215.7 \text{ A m}^{-2}$ ), respectively. The enhanced  $G_{\max}$  reveals the reduced charge recombination at the interface between the perovskite and  $\text{NiO}_x$  layers after FDA modification. The carrier transport and collection probabilities at any effective voltage can be directly obtained from the ratio of  $J_{\text{ph}}/J_{\text{sat}}$ . The carrier transport and collection probability of cells with FDA modification was increased to 98.4% from 88.2% in control cells, indicating that FDA modification can efficiently improve hole transport and collection abilities of the cells.<sup>29,37</sup>

To further investigate the mechanism of the FDA modified  $\text{NiO}_x$  layer, electrochemical impedance spectra of cells with and without FDA modification were measured. Nyquist plots of the cells without FDA modification exhibit an arc in the fourth quadrant in the low frequency range, as shown in Fig. 5a, indicating that negative capacitance exists in PSCs with a pure  $\text{NiO}_x$  layer. However, the  $-Z''$  values are always positive at any voltages and frequencies after modification with FDA, as shown in Fig. 5b. The negative capacitive behavior is related to the massive accumulation of carriers at the interfaces due to the Schottky contact.<sup>38</sup> The negative capacitive behavior of the cells can be controlled through reducing the interface barrier or forming ohmic contacts using an interface modification material.<sup>32,39,40</sup> Therefore, the controlled negative capacitive behavior in PSCs with the FDA modified  $\text{NiO}_x$  layer is attributed to the reduced carrier accumulation at the interface of the  $\text{NiO}_x$ /perovskite due to the superior contact properties. The Bode-phase plots of PSCs with and without FDA modification at a bias voltage of 0.9 V are shown in Fig. 5c. The frequency response peak of PSCs with pristine

$\text{NiO}_x$  becomes obvious when compared to PSCs with  $\text{NiO}_x$ /FDA, which may be divided into two peaks by curve fitting. The characteristic frequencies of low-frequency and high-frequency sides are related to carrier recombination and carrier diffusion, respectively. The peak frequency of the low-frequency side is shifted to a lower region with the FDA modified  $\text{NiO}_x$  layer, indicating a reduced carrier recombination due to the passivation effect of FDA and the better crystallization of the perovskite layer.<sup>41</sup> The capacitance–voltage characteristics at 1 kHz are shown in Fig. 5d. The capacitance effect was gradually increased with increasing bias voltage, which is indicative of charge accumulation at the interface.<sup>42,43</sup> With FDA modification, the capacitance of the cells is significantly reduced, further confirming the passivation effect of FDA and improved contact properties.<sup>42,44</sup> The lower accumulation of charge carriers helps obtaining higher photocurrent and less  $J$ - $V$  hysteresis.<sup>45</sup>

The  $J$ - $V$  curves of PSCs with and without FDA modification as a function of light intensity are shown in Fig. S3.† The linearly fitting curves of the photovoltaic parameters *versus* light intensity are shown in Fig. 6. The slopes of  $1.58k_{\text{B}}T/q$  and  $1.66k_{\text{B}}T/q$  (where  $k_{\text{B}}$  is the Boltzmann constant,  $T$  is the absolute temperature, and  $q$  is the elementary charge) were simulated for FDA modified cells and the control cells, which are obviously larger than  $k_{\text{B}}T/q$ , indicating that the recombination mechanisms of trap-assisted recombination and bimolecular recombination both play an important role in PSCs with and without FDA modification.<sup>46,47</sup> However, the relative lower deviation slope for FDA modified PSCs suggested the reduced trap-assisted recombination due to FDA passivation. The FF of both kinds of PSCs almost remain constant at a low light density, but the FF values of PSCs without FDA are more obviously decreased at a higher light density, which is evidence of a heavy influence of trap-assisted recombination.<sup>47</sup> The slightly linear deviation of  $J_{\text{ph}}$  of cells with light intensity

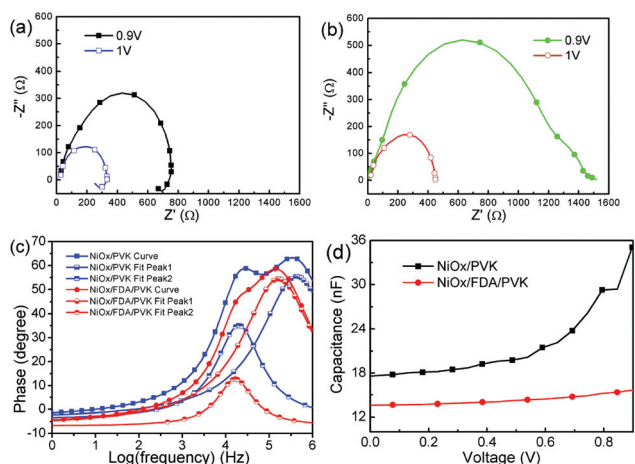


**Fig. 5** Nyquist plots of PSCs based on  $\text{NiO}_x$  with (a) and without (b) FDA modification at the forward bias voltage of 0.9 V and 0.1 V in the dark; (c) Bode-phase plots of PSCs with  $\text{NiO}_x$  and  $\text{NiO}_x$ /FDA HTLs at the bias voltage of 0.9 V; (d) capacitance–voltage characteristics of cells with and without FDA modification.

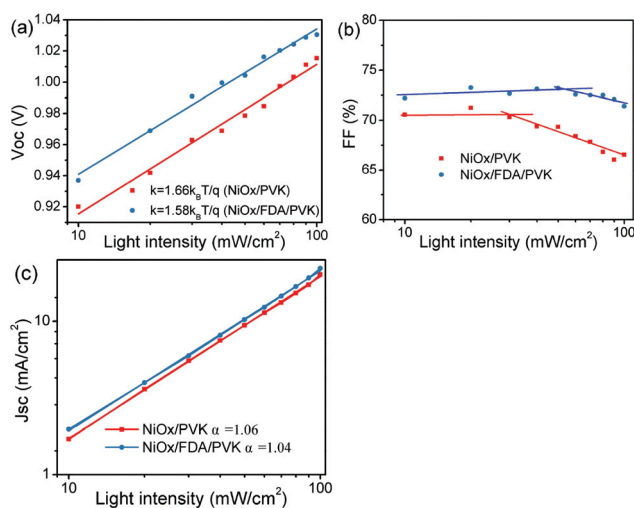


**Fig. 6**  $V_{\text{oc}}$ , FF and  $J_{\text{sc}}$  as a function of light density for PSCs with  $\text{NiO}_x$  and  $\text{NiO}_x$ /FDA. The FDA concentration of the modified spin-coated  $\text{NiO}_x$  surface is  $0.1 \text{ mg ml}^{-1}$ .

also supported a certain role of trap-assisted recombination, which is partly responsible for lower integrated  $J_{sc}$  than  $J_{sc}$  from  $J-V$  curves.<sup>30,47</sup>

Solar cells containing organic materials or groups, for example organic solar cells and perovskite solar cells, can be quickly deteriorated under UV irradiation.<sup>48</sup> The present light durability tests of perovskite solar cells are usually filtered ultraviolet light to avoid UV damage.<sup>11</sup> However, the enhanced UV durability of perovskite solar cells is still an important aim to improve the lifetime of cells. UV irradiation can cause fast release of  $O_2$  on the  $TiO_2$  and ZnO surface, and induces a large amount of deep trap states leading to charge recombination,<sup>31,42</sup> which accelerates the degradation of the  $TiO_2$ /perovskite interface<sup>49</sup> and the ZnO/organic photoactive layer.<sup>48</sup> Therefore, PSCs using  $NiO_x$  as the HTL with and without FDA modification were investigated for comparison. A UV-assisted acceleration aging test of eight devices of each type of PSC without encapsulation under a relative humidity (RH) of 40% in air was carried out to evaluate UV durability. The photovoltaic parameters of PSCs with and without FDA modification at different exposure times of UV irradiation are shown in Fig. 7. The original PCEs of selected PSCs with and without FDA modification are close to the average PCEs of each type. The parameters including the PCE, FF,  $J_{sc}$ , and  $V_{oc}$  for PSCs without FDA modification were more quickly deteriorated in the UV-assisted acceleration aging test. The normalized PCE of the reference PSCs was quickly decreased to 3.8% the original PCE value and the cells almost disappeared after UV exposure for 24 hours. However, PSCs with FDA modification still maintained the original PCE value of 49.8%, showing superior UV durability. Considering the similar transmittance of spectra for  $NiO_x$  films modified with and without FDA, the enhanced UV durability of PSCs is not attributed to the enhanced UV absorption of FDA, although the effect of improved UV-resistance of

PSCs cannot be excluded completely due to the strong UV absorption properties of FDA. The improved UV-resistance of PSCs is primarily attributed to the passivation effect of FDA and the better crystallization of the perovskite, which is consistent with the previous report that the passivation of  $TiO_2$  surfaces can improve the stability of perovskite solar cells, including better UV-resistance.<sup>42</sup>

Considering the success of organic solar cells with FDA inserted between ITO and the n-type ZnO layer,<sup>21</sup> we also investigated the performance of PSCs with FDA inserted at the interface of the perovskite/PCBM layers, as shown in Fig. S4.† The photovoltaic parameters of PSCs are summarized in Table S2.† The PCE of PSCs with a FDA/PCBM layer can reach 16.62%, which is obviously higher than the PCE of reference cells. The reverse saturation dark current density of PSCs with FDA/PCBM was inhibited and their rectifying property was improved. Furthermore, the disappeared negative capacitance of cells with FDA/PCBM at any voltages and frequencies was observed, as shown in Fig. S5b,† indicating that the carrier recombination and accumulation phenomena at the perovskite/PCBM interface can be obviously inhibited due to the interfacial modification of FDA, which results in the improvement of the FF and  $J_{sc}$  of PSCs. The characteristic frequency of the low-frequency side for PSCs with the FDA/PCBM electron transport layer is also shifted to a lower region compared to the reference cells, as shown in Fig. S5c,† which is attributed to the reduced carrier recombination.<sup>41</sup> This result indicates that FDA also has the passivation function of the perovskite layer, which can reduce the surface defects of the perovskite layer. The carboxyl groups ( $-COOH$ ) of FDA usually exhibit stronger interactions with Pb ions or I ions of the perovskite compared with PCBM due to the interactions of hydrogen bonds, which can passivate the surface of the perovskite layer.<sup>50</sup> Meanwhile, the enhanced conductivity of PCBM modified with FDA compared to pure PCBM can further improve electron carrier transport and collection abilities. Therefore, these comprehensive functions are expected to be responsible for the reduced electron carrier recombination and accumulation at the interface of the perovskite/PCBM.

To directly demonstrate enhanced transport and collection abilities of the FDA modified n-type layer, the FDA solution with  $0.1 \text{ mg ml}^{-1}$  was spin-coated onto the AZO surface. The  $J-V$  curves and  $J_{ph}-V_{eff}$  curves of PTB7-Th:PC71BM based polymer solar cells with AZO modified with and without FDA are shown in Fig. 8. The PCE of the polymer solar cells with AZO/FDA were greatly increased to 9.86% from 8.27% of the control cells. The carrier transport and collecting probabilities of the polymer solar cells with the FDA modified layer were increased to 90.9% from 88.4% in control cells, and the corresponding reduced reverse dark current of the polymer solar cells with FDA modification can be observed, indicating that FDA as an n-type AZO modification layer can also efficiently improve electron transport and collection abilities and inhibit the carrier recombination.<sup>29</sup> Therefore, these results indicate that the FDA modified layer has dual functions in modifying hole and electron transport layers.

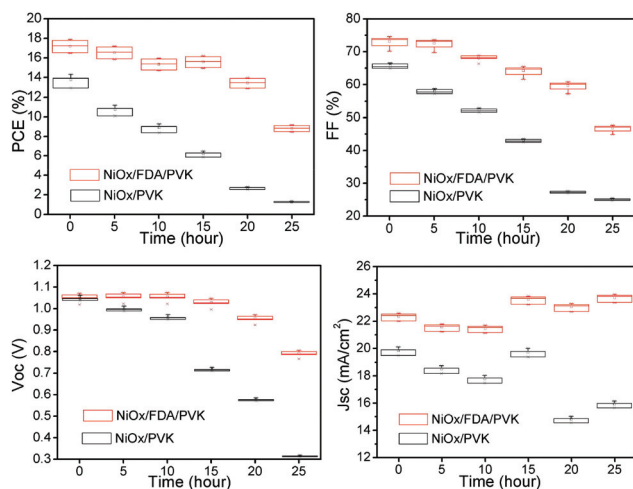
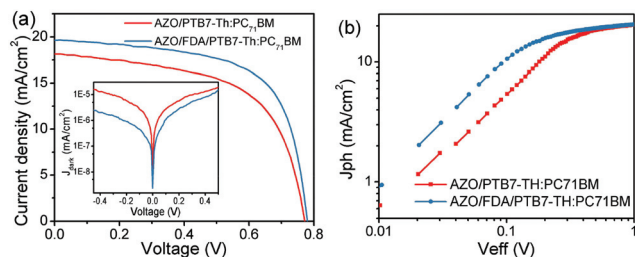
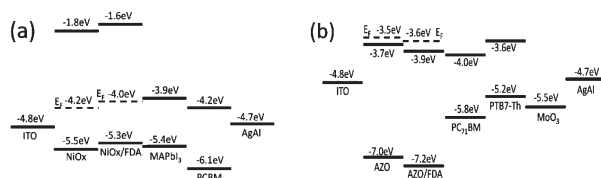


Fig. 7 PCE, FF,  $V_{oc}$  and  $J_{sc}$  of PSCs with and without FDA modification without encapsulation at different UV exposure times with an RH of 40% in air. The exposed wavelength of UV tubes is 365 nm and UV light density is  $13 \text{ mW cm}^{-2}$ .



**Fig. 8** (a)  $J$ - $V$  curves of polymer solar cells modified with and without FDA. Dark  $J$ - $V$  curves of the corresponding cells (inset); (b) plots of  $J_{ph}$  versus  $V_{eff}$  for polymer solar cells with and without FDA modification. The structure of cells: ITO/AZO (20 nm)/FDA/PTB7-Th:PC71BM (80 nm)/MoO<sub>3</sub> (7 nm)/AgAl.



**Fig. 9** Energy level diagrams of the perovskite and polymer solar cells. (a) Perovskite solar cells based on NiO<sub>x</sub> modified with and without the FDA layer; (b) polymer solar cells based on AZO modified with and without the FDA layer.

To further explain the reason that the FDA modified layer has dual functions in improving hole and electron transport abilities, the band alignment diagrams of related layers are summarized in Fig. 9. The Fermi energy level ( $E_F$ ), valence band ( $V_b$ ) and conduction band ( $V_c$ ) for NiO<sub>x</sub> and AZO with and without the FDA modified layer were calibrated through UPS measurements and its optical band gap, as shown in Fig. S6.† The energy band gaps of NiO<sub>x</sub> and AZO films are respectively 3.7 eV and 3.3 eV, calibrated from their absorption spectra. The  $E_F$  value of NiO<sub>x</sub> modified with the FDA layer is increased to  $-4.0$  eV from  $-4.2$  eV of pristine NiO<sub>x</sub>, which boosts hole transport from the perovskite layer to the NiO<sub>x</sub> layer due to the reduced contact barrier. Similarly, the  $E_F$  value of AZO modified with the FDA layer is reduced to  $-3.6$  eV from  $-3.5$  eV of pristine AZO, which can lead to the reduced contact barrier and boost electron transport from PC<sub>71</sub>BM to the AZO layer. Therefore, the varied trend of the Fermi energy levels of NiO<sub>x</sub> and AZO after FDA modification further supports the dual functions of FDA modification to increase hole and electron transport and exaction abilities.

## 4. Conclusions

In summary, the champion PCEs of PSCs with FDA modified NiO<sub>x</sub> and PCBM transport layers can respectively reach 18.20% and 16.62%, which is obviously higher than the PCE (15.13%) of PSCs with pure NiO<sub>x</sub>, indicating that using FDA as the hole and electron transport modified layer is a good strategy to

efficiently improve the performance of PSCs. The integrated effects of better crystallization of the perovskite layer, the passivation effect of FDA, and the improved electrical conductivity of FDA modified NiO<sub>x</sub> and superior interface contact properties at the interface of NiO<sub>x</sub>/perovskite layers after FDA modification are primarily responsible for high PCEs, the hysteresis-free effect and UV durability of PSCs. Therefore, ferrocene derivatives as a NiO<sub>x</sub> modified layer are a class material with great potential to improve the PCEs and UV-resistance of PSCs.

## Conflicts of interest

There are no conflicts to declare.

## Acknowledgements

This work was supported by the National Natural Science Foundation of China (grant No. 61275038 and 11274119).

## Notes and references

- 1 NREL Best Research-Cell Efficiencies; Available from: <https://www.nrel.gov/pv/assets/images/efficiency-chart.png> (accessed Jan 2018).
- 2 H. Luo, X. Lin, X. Hou, L. Pan, S. Huang and X. Chen, Efficient and Air-Stable Planar Perovskite Solar Cells Formed on Graphene-Oxide-Modified PEDOT:PSS Hole Transport Layer, *Nano-Micro Lett.*, 2017, **9**(4), 39.
- 3 M. Jørgensen, K. Norrman and F. C. Krebs, Stability/degradation of polymer solar cells, *Sol. Energy Mater. Sol. Cells*, 2008, **92**(7), 686–714.
- 4 S. Ye, W. Sun, Y. Li, W. Yan, H. Peng, Z. Bian, Z. Liu and C. Huang, CuSCN-Based Inverted Planar Perovskite Solar Cell with an Average PCE of 15.6%, *Nano Lett.*, 2015, **15**(6), 3723–3728.
- 5 J. A. Christians, R. C. M. Fung and P. V. Kamat, An Inorganic Hole Conductor for Organo-Lead Halide Perovskite Solar Cells. Improved Hole Conductivity with Copper Iodide, *J. Am. Chem. Soc.*, 2014, **136**(2), 758–764.
- 6 A. E. Shalan, T. Oshikiri, S. Narra, M. M. Elshanawany, K. Ueno, H.-P. Wu, K. Nakamura, X. Shi, E. W.-G. Diao and H. Misawa, Cobalt Oxide (CoOx) as an Efficient Hole-Extracting Layer for High-Performance Inverted Planar Perovskite Solar Cells, *ACS Appl. Mater. Interfaces*, 2016, **8**(49), 33592–33600.
- 7 J. Y. Jeng, K. C. Chen, T. Y. Chiang, P. Y. Lin, T. D. Tsai, Y. C. Chang, T. F. Guo, P. Chen, T. C. Wen and Y. J. Hsu, Nickel Oxide Electrode Interlayer in CH<sub>3</sub>NH<sub>3</sub>PbI<sub>3</sub> Perovskite/PCBM Planar-Heterojunction Hybrid Solar Cells, *Adv. Mater.*, 2014, **26**(24), 4107–4113.
- 8 T. A. N. Peiris, A. K. Baranwal, H. Kanda, S. Fukumoto, S. Kanaya, L. Cojocar, T. Bessho, T. Miyasaka, H. Segawa and S. Ito, Enhancement of the hole conducting effect of

- NiO by a N<sub>2</sub> blow drying method in printable perovskite solar cells with low-temperature carbon as the counter electrode, *Nanoscale*, 2017, **9**(17), 5475–5482.
- 9 J. H. Kim, P. W. Liang, S. T. Williams, N. Cho, C. C. Chueh, M. S. Glaz, D. S. Ginger and A. K. Y. Jen, High-Performance and Environmentally Stable Planar Heterojunction Perovskite Solar Cells Based on a Solution-Processed Copper-Doped Nickel Oxide Hole-Transporting Layer, *Adv. Mater.*, 2015, **27**(4), 695–701.
- 10 W. Chen, Y. Wu, Y. Yue, J. Liu, W. Zhang, X. Yang, H. Chen, E. Bi, I. Ashraful, M. Grätzel and L. Han, Efficient and stable large-area perovskite solar cells with inorganic charge extraction layers, *Science*, 2015, **350**(6263), 944.
- 11 Y. Wu, X. Yang, W. Chen, Y. Yue, M. Cai, F. Xie, E. Bi, A. Islam and L. Han, Perovskite solar cells with 18.21% efficiency and area over 1 cm<sup>2</sup> fabricated by heterojunction engineering, *Nat. Energy*, 2016, **1**, 16148.
- 12 R. Fan, Y. Huang, L. Wang, L. Li, G. Zheng and H. Zhou, The Progress of Interface Design in Perovskite-Based Solar Cells, *Adv. Energy Mater.*, 2016, **6**(17), 1600460.
- 13 Y. Hou, W. Chen, D. Baran, T. Stubhan, N. A. Luechinger, B. Hartmeier, M. Richter, J. Min, S. Chen, C. O. R. Quiroz, N. Li, H. Zhang, T. Heumueller, G. J. Matt, A. Osvet, K. Forberich, Z. G. Zhang, Y. Li, B. Winter, P. Schweizer, E. Spiecker and C. J. Brabec, Overcoming the Interface Losses in Planar Heterojunction Perovskite-Based Solar Cells, *Adv. Mater.*, 2016, **28**(25), 5112–5120.
- 14 Y. Bai, H. Chen, S. Xiao, Q. Xue, T. Zhang, Z. Zhu, Q. Li, C. Hu, Y. Yang, Z. Hu, F. Huang, K. S. Wong, H.-L. Yip and S. Yang, Effects of a Molecular Monolayer Modification of NiO Nanocrystal Layer Surfaces on Perovskite Crystallization and Interface Contact toward Faster Hole Extraction and Higher Photovoltaic Performance, *Adv. Funct. Mater.*, 2016, **26**(17), 2950–2958.
- 15 Y. Shao, Z. Xiao, C. Bi, Y. Yuan and J. Huang, Origin and elimination of photocurrent hysteresis by fullerene passivation in CH<sub>3</sub>NH<sub>3</sub>PbI<sub>3</sub> planar heterojunction solar cells, *Nat. Commun.*, 2014, **5**, 5784.
- 16 D. L. Staebler and C. R. Wronski, Optically induced conductivity changes in discharge-produced hydrogenated amorphous silicon, *J. Appl. Phys.*, 1980, **51**(6), 3262–3268.
- 17 J. M. Frost, K. T. Butler, F. Brivio, C. H. Hendon, M. van Schilfgaarde and A. Walsh, Atomistic origins of high-performance in hybrid halide perovskite solar cells, *Nano Lett.*, 2014, **14**(5), 2584–2590.
- 18 A. Dualeh, T. Moehl, N. Tétreault, J. Teuscher, P. Gao, M. K. Nazeeruddin and M. Grätzel, Impedance Spectroscopic Analysis of Lead Iodide Perovskite-Sensitized Solid-State Solar Cells, *ACS Nano*, 2014, **8**(1), 362–373.
- 19 P. Steffen, C. Unkelbach, M. Christmann, W. Hiller and C. Strohmam, Catalytic and stereoselective ortho-lithiation of a ferrocene derivative, *Angew. Chem., Int. Ed.*, 2013, **52**(37), 9836–9840.
- 20 L. Fernández and H. Carrero, Electrochemical evaluation of ferrocene carboxylic acids confined on surfactant–clay modified glassy carbon electrodes: oxidation of ascorbic acid and uric acid, *Electrochim. Acta*, 2005, **50**(5), 1233–1240.
- 21 B. Li, T. Jiu, C. Kuang, Q. Chen, S. Ma, J. Li, X. Hou and J. Fang, Improving the efficiency of inverted organic solar cells by introducing ferrocenedicarboxylic acid between an ITO/ZnO interlayer, *RSC Adv.*, 2016, **6**(38), 32000–32006.
- 22 W. Yang, Y. Yao and C.-Q. Wu, Origin of the high open circuit voltage in planar heterojunction perovskite solar cells: Role of the reduced bimolecular recombination, *J. Appl. Phys.*, 2015, **117**(9), 095502.
- 23 M. A. Mahmud, N. K. Elumalai, M. B. Upama, D. Wang, L. Zarei, V. R. Goncales, M. Wright, C. Xu, F. Haque and A. Uddin, Adsorbed carbon nanomaterials for surface and interface-engineered stable rubidium multi-cation perovskite solar cells, *Nanoscale*, 2018, **10**(2), 773–790.
- 24 K. Wang, W. Zhao, J. Liu, J. Niu, Y. Liu, X. Ren, J. Feng, Z. Liu, J. Sun, D. Wang and S. F. Liu, CO<sub>2</sub> Plasma-Treated TiO<sub>2</sub> Film as an Effective Electron Transport Layer for High-Performance Planar Perovskite Solar Cells, *ACS Appl. Mater. Interfaces*, 2017, **9**(39), 33989–33996.
- 25 M. A. Peck and M. A. Langell, Comparison of Nanoscaled and Bulk NiO Structural and Environmental Characteristics by XRD, XAFS, and XPS, *Chem. Mater.*, 2012, **24**(23), 4483–4490.
- 26 W. Chen, F.-Z. Liu, X.-Y. Feng, A. B. Djurišić, W. K. Chan and Z.-B. He, Cesium Doped NiOx as an Efficient Hole Extraction Layer for Inverted Planar Perovskite Solar Cells, *Adv. Energy Mater.*, 2017, **7**(19), 1700722.
- 27 S. Seo, I. J. Park, M. Kim, S. Lee, C. Bae, H. S. Jung, N.-G. Park, J. Y. Kim and H. Shin, An ultra-thin, un-doped NiO hole transporting layer of highly efficient (16.4%) organic-inorganic hybrid perovskite solar cells, *Nanoscale*, 2016, **8**(22), 11403–11412.
- 28 M. Li, B. Li, G. Cao and J. Tian, Monolithic MAPbI<sub>3</sub> films for high-efficiency solar cells via coordination and a heat assisted process, *J. Mater. Chem. A*, 2017, **5**(40), 21313–21319.
- 29 X. Jia, Z. Jiang, X. Chen, J. Zhou, L. Pan, F. Zhu, Z. Sun and S. Huang, Highly Efficient and Air Stable Inverted Polymer Solar Cells Using LiF-Modified ITO Cathode and MoO<sub>3</sub>/AgAl Alloy Anode, *ACS Appl. Mater. Interfaces*, 2016, **8**(6), 3792–3799.
- 30 Z. Jiang, X. Chen, X. Lin, X. Jia, J. Wang, L. Pan, S. Huang, F. Zhu and Z. Sun, Amazing stable open-circuit voltage in perovskite solar cells using AgAl alloy electrode, *Sol. Energy Mater. Sol. Cells*, 2016, **146**, 35–43.
- 31 W. Li, W. Zhang, S. Van Reenen, R. J. Sutton, J. Fan, A. A. Haghighirad, M. B. Johnston, L. Wang and H. J. Snaith, Enhanced UV-light stability of planar heterojunction perovskite solar cells with caesium bromide interface modification, *Energy Environ. Sci.*, 2016, **9**(2), 490–498.
- 32 F. Zhu, X. Chen, Z. Lu, J. Yang, S. Huang and Z. Sun, Efficiency Enhancement of Inverted Polymer Solar Cells Using Ionic Liquid-functionalized Carbon Nanoparticles-modified ZnO as Electron Selective Layer, *Nano-Micro Lett.*, 2014, **6**(1), 24–29.

- 33 M. Li, X. Yan, Z. Kang, X. Liao, Y. Li, X. Zheng, P. Lin, J. Meng and Y. Zhang, Enhanced Efficiency and Stability of Perovskite Solar Cells via Anti-Solvent Treatment in Two-Step Deposition Method, *ACS Appl. Mater. Interfaces*, 2017, **9**(8), 7224–7231.
- 34 D. Song, J. Ji, Y. Li, G. Li, M. Li, T. Wang, D. Wei, P. Cui, Y. He and J. M. Mbengue, Degradation of organometallic perovskite solar cells induced by trap states, *Appl. Phys. Lett.*, 2016, **108**(9), 093901.
- 35 D. Song, P. Cui, T. Wang, D. Wei, M. Li, F. Cao, X. Yue, P. Fu, Y. Li, Y. He, B. Jiang and M. Trevor, Managing Carrier Lifetime and Doping Property of Lead Halide Perovskite by Postannealing Processes for Highly Efficient Perovskite Solar Cells, *J. Phys. Chem. C*, 2015, **119**(40), 22812–22819.
- 36 M.-F. Xu, X.-Z. Zhu, X.-B. Shi, J. Liang, Y. Jin, Z.-K. Wang and L.-S. Liao, Plasmon Resonance Enhanced Optical Absorption in Inverted Polymer/Fullerene Solar Cells with Metal Nanoparticle-Doped Solution-Processable TiO<sub>2</sub> Layer, *ACS Appl. Mater. Interfaces*, 2013, **5**(8), 2935–2942.
- 37 J. Wang, X. Jia, J. Zhou, L. Pan, S. Huang and X. Chen, Improved Performance of Polymer Solar Cells by Thermal Evaporation of AgAl Alloy Nanostructures into the Hole-Transport Layer, *ACS Appl. Mater. Interfaces*, 2016, **8**(39), 26098–26104.
- 38 G. Garcia-Belmonte, A. Munar, E. M. Barea, J. Bisquert, I. Ugarte and R. Pacios, Charge carrier mobility and lifetime of organic bulk heterojunctions analyzed by impedance spectroscopy, *Org. Electron.*, 2008, **9**(5), 847–851.
- 39 X. Chen, J. Yang, J. Lu, K. K. Manga, K. P. Loh and F. Zhu, Ionic liquid-functionalized carbon nanoparticles-modified cathode for efficiency enhancement in polymer solar cells, *Appl. Phys. Lett.*, 2009, **95**(13), 133305.
- 40 F. Zhu, X. Chen, L. Zhou, J. Zhou, J. Yang, S. Huang and Z. Sun, Dependence of the performance of inverted polymer solar cells on thickness of an electron selective ZnO layer deposited by magnetron sputtering, *Thin Solid Films*, 2014, **551**, 131–135.
- 41 G. Perrier, R. de Bettignies, S. Berson, N. Lemaître and S. Guillerez, Impedance spectrometry of optimized standard and inverted P3HT-PCBM organic solar cells, *Sol. Energy Mater. Sol. Cells*, 2012, **101**, 210–216.
- 42 Y. Li, Y. Zhao, Q. Chen, Y. M. Yang, Y. Liu, Z. Hong, Z. Liu, Y. T. Hsieh, L. Meng, Y. Li and Y. Yang, Multifunctional Fullerene Derivative for Interface Engineering in Perovskite Solar Cells, *J. Am. Chem. Soc.*, 2015, **137**(49), 15540–15547.
- 43 K. Wojciechowski, S. D. Stranks, A. Abate, G. Sadoughi, A. Sadhanala, N. Kopidakis, G. Rumbles, C.-Z. Li, R. H. Friend, A. K. Y. Jen and H. J. Snaith, Heterojunction Modification for Highly Efficient Organic–Inorganic Perovskite Solar Cells, *ACS Nano*, 2014, **8**(12), 12701–12709.
- 44 K. Schwanitz, U. Weiler, R. Hunger, T. Mayer and W. Jaegermann, Synchrotron-Induced Photoelectron Spectroscopy of the Dye-Sensitized Nanocrystalline TiO<sub>2</sub>/Electrolyte Interface: Band Gap States and Their Interaction with Dye and Solvent Molecules, *J. Phys. Chem. C*, 2007, **111**(2), 849–854.
- 45 H. Zhang, C. Liang, Y. Zhao, M. Sun, H. Liu, J. Liang, D. Li, F. Zhang and Z. He, Dynamic interface charge governing the current-voltage hysteresis in perovskite solar cells, *Phys. Chem. Chem. Phys.*, 2015, **17**(15), 9613–9618.
- 46 S. R. Cowan, A. Roy and A. J. Heeger, Recombination in polymer-fullerene bulk heterojunction solar cells, *Phys. Rev. B: Condens. Matter*, 2010, **82**(24), 245207.
- 47 C. M. Proctor, C. Kim, D. Neher and T.-Q. Nguyen, Nongeminate Recombination and Charge Transport Limitations in Diketopyrrolopyrrole-Based Solution-Processed Small Molecule Solar Cells, *Adv. Funct. Mater.*, 2013, **23**(28), 3584–3594.
- 48 X. Lin, H. Luo, X. Jia, J. Wang, J. Zhou, Z. Jiang, L. Pan, S. Huang and X. Chen, Efficient and ultraviolet durable inverted polymer solar cells using thermal stable GZO-AgTi-GZO multilayers as a transparent electrode, *Org. Electron.*, 2016, **39**, 177–183.
- 49 T. Leijtens, G. E. Eperon, S. Pathak, A. Abate, M. M. Lee and H. J. Snaith, Overcoming ultraviolet light instability of sensitized TiO<sub>2</sub> with meso-superstructured organometal tri-halide perovskite solar cells, *Nat. Commun.*, 2013, **4**, 2885.
- 50 X. Hou, S. Huang, W. Ou-Yang, L. Pan, Z. Sun and X. Chen, Constructing Efficient and Stable Perovskite Solar Cells via Interconnecting Perovskite Grains, *ACS Appl. Mater. Interfaces*, 2017, **9**(40), 35200–35208.